Design of mutually coupled circuit employing voltage differencing transconductance amplifiers (VDTAs)

Fatih SAYDAM (fatih.saydam@ogr.iuc.edu.tr)
Istanbul University-Cerrahpaşa
Fırat KAÇAR
Istanbul University-Cerrahpaşa
Emre ÖZER
Istanbul University-Cerrahpaşa

Research Article

Keywords: VDTA, mutually coupled circuit, electronically tunable, active device

Posted Date: April 6th, 2022

DOI: https://doi.org/10.21203/rs.3.rs-1507836/v1

Design of mutually coupled circuit employing voltage differencing transconductance amplifiers (VDTAs)

Fatih SAYDAM[1,*] fatih.saydam@ogr.iuc.edu.tr
Fırat KAÇAR[1] fkacar@istanbul.edu.tr
Emre ÖZER[2] emreozer@istanbul.edu.tr

[1]Department of Electrical and Electronics Engineering, Istanbul University-Cerrahpaşa, 34320, Avcilar, Istanbul, Turkey

[2]Department of Electrical and Energy, Istanbul University-Cerrahpaşa, 34500 Buyukcekmece, Istanbul, Turkey

* Corresponding Author

Abstract: This paper presents a new mutually coupled circuit (MCC) employing voltage differencing transconductance amplifiers (VDTAs), firstly. The proposed circuit consists of two VDTAs, two grounded capacitors, and a single resistor. The inductances can be adjusted independently and electronically. Only one matching condition is required to achieve symmetrical coupling. The time-domain and frequency-domain simulation results confirm the theoretical analysis. An application example is given to demonstrate the functionality of the circuit.

Keywords: VDTA, mutually coupled circuit, electronically tunable, active device.

1. Introduction

Mutual coupled circuits (MCC), also called as synthetic transformers, are extensively used in several fields; for instance, analog communication, signal processing, instrumentation, control engineering, measurement etc. Hence, there are a lot of MCC designs in technical literature. Firstly, MCC has been developed with op-amps by Atiya [1], Soderstrand [2], Higashimura and Fukui [3]. These designs are limited in some ways, for instance, low slew rate. Because of the low slew rate, op-amps are adversely affected to high frequency applications. Furthermore, designs that including op-amps have restricted bandwidth and constant gain-bandwidth. Operational transconductance amplifier (OTA) based MCC has been executed by Higashimura and Fukui [4], [5]. These designs have eight OTAs and two capacitors. Higashimura and Fukui [5] also reported realization of current conveyor based MCC in same paper. In this circuit eight CCIIs as active element and six resistors and four capacitors as passive element existing. Shigehiro et al. [6] have been proposed a BJT based MCC design that includes twelve BJT, thirty-two resistors and four capacitors. Another BJT based MCC has been realized by

Nakamura et al. [7] with eight BJTs, ten resistors and four capacitors. Abuelma'atti et al. [8] have proposed a MCC that contains six CCIIs as active component; six resistors and two capacitors as passive component. Yuce et al. [9] have reported a MCC that operates with four CCIIs, five resistors and two capacitors. Including three CCCIIs, two DO-CCCIIs and two CCIIs design has been realized by Yuce and Minaei [10]. This product has five passive components that two grounded resistors and three grounded capacitors. In this report, alongside transformer simulator, low-pass and high-pass ladder filter application has been realized. After that another MCC design has been executed by Yuce and Minaei [11] that consists in four CCCIIs and five resistors and two capacitors. Gunes et al. [12] proposed the design that includes four operational amplifiers (OTAs) as active components and two grounded resistors and two grounded capacitors as passive components. They also reported another MCC, including two DVCCs and two CCIIs in same paper. CC-CBTA based MCC designed has been realized by Koksal et al. [13]. That design consists with three active components as CC-CBTAs and three passive components as grounded capacitors without external resistor. In this proposed MCC, values of inductances can be adjusted by altering the bias current of CC-CBTA. Pandey et al. [14] have reported MCC that includes two DVCCCTAs, one grounded resistors and two grounded capacitors. Inductances of this circuit can be controlled with biasing currents of active components besides mutual coupling can be adjusted with value of grounded resistor. Containing two CC-CCTAs, one resistor and one capacitor circuit has been proposed by Sagbas [15]. Sagbas at al. [16] have reported current backward transconductance amplifier (CBTA) based MCC. This circuit has been realized with two CBTAs, three resistors and two capacitors. Including four CFOAs, five resistors and two capacitors MCC production has been proposed by Dogan et al. [17]. Finally voltage differencing current conveyor (VDCC) based MCC design has been realized by Ozer and Kacar [18]. This design includes three resistors and two capacitors. Some information of the proposed MCCs is given in Table 1.

In this work, a new mutual coupled circuit is proposed employing two VDTAs as active component and two grounded capacitors and only grounded resistor as passive components. The proposed circuit can be electronically tunable with VDTA biasing currents. Values of the primary self-inductance, the secondary self-inductance and the mutual inductance can be adjusted separately. Coefficient of coupling can be controlled with grounded resistor to changing the inductances for desired values. In order to observation of the proposed MCC, some analysis has been realized with DTBP filter application by using LTspice program.

Table 1 Comparison of MCCs

References	Year	# and type of active components	# of resistors (Grounded)	# of capacitors (Grounded)	Operating frequency	Electronically tunable
Atiya [1]	1978	2 Op-amps	0	3 (2)	N/A	No
Soderstrand [2]	1978	2 Op-amps	5 (1)	0	N/A	No
Higashimura and Fukui [3]	1985	4 Op-amps	9 (1)	2 (0)	Up to 1.4 kHz	No
Higashimura and Fukui [4]	1991	8 OTAs	0	2 (2)	N/A	Yes
Higashimura and Fukui [5]	1991	8 OTAs	0	2 (2)	N/A	Yes
Higashimura and Fukui [5]	1991	8 CCIIs	6 (4)	4 (4)	Up to 3.3 kHz	No
Shigehiro et al. [6]	1991	12 BJTs	32 (16)	4 (4)	Up to 10 MHz	No
Nakamura et al. [7]	1996	8 BJTs	10 (5)	4 (4)	Up to 500 kHz	No
Abuelma'atti et al. [8]	2005	6 CCIIs	6 (4)	2 (2)	Up to 15 MHz	No
Yuce et al. [9]	2007	4 CCIIs	5 (3)	2 (2)	Up to 2.5 kHz	No
Yuce and Minaei [10]	2007	3 CCCIIs 2 DO-CCCIIs 2 CCIIs	2 (2)	3 (3)	Up to 300 kHz	Yes
Yuce and Minaei [11]	2007	4 CCCIIs	5 (3)	2 (2)	Up to 4 kHz	No
Gunes et al. [12]	2011	4 OTAs	2 (2)	2 (2)	Up to 100 kHz	Yes
Gunes et al. [12]	2011	2 DVCCs 2 CCIIs	6 (6)	2 (2)	Up to 100 MHz	No
Koksal et al. [13]	2012	3 CC-CBTAs	0	3 (3)	Up to 100 MHz	Yes
Pandey et al. [14]	2012	2 DVCCCTAs	1 (1)	2 (2)	Up to 20 MHz	Yes
Sagbas [15]	2014	2 CC-CCTAs	1 (1)	2 (2)	Up to 1 MHz	Yes
Sagbas at al. [16]	2017	2 CBTAs	3 (1)	2 (2)	Up to 10 MHz	Yes
Dogan et al. [17]	2020	4 CFOAs	5 (1)	2 (2)	Up to 100 MHz	No
Ozer and Kacar [18]	2021	2 VDCCs	3 (1)	2 (2)	Up to 100 MHz	Yes
In this work	2022	2 VDTAs	1 (1)	2 (2)	Up to 500 MHz	Yes

2. The proposed circuit

Terminal relations of VDTA, whose circuit symbol is given in Fig. 1, are expressed with the following equation.

$$\begin{bmatrix} I_P \\ I_N \\ I_{ZP} \\ I_{ZN} \\ I_{X_+} \\ I_{X_-} \end{bmatrix} = \begin{bmatrix} 0 & 0 & 0 & 0 & 0 & 0 \\ 0 & 0 & 0 & 0 & 0 & 0 \\ g_{mF} & -g_{mF} & 0 & 0 & 0 & 0 \\ -g_{mF} & g_{mF} & 0 & 0 & 0 & 0 \\ 0 & 0 & g_{mS} & 0 & 0 & 0 \\ 0 & 0 & -g_{mS} & 0 & 0 & 0 \end{bmatrix} \begin{bmatrix} V_P \\ V_N \\ V_{ZP} \\ V_{ZN} \\ V_{X_+} \\ V_{X_-} \end{bmatrix} \quad (1)$$

The transconductance gains g_{mF} and g_{mS} are given by:

$$g_{mF} = \left(\frac{g_3 + g_4}{2}\right) \quad (2)$$

$$g_{mS} = \left(\frac{g_5 + g_8}{2}\right) \quad (3)$$

where $g_i = \sqrt{I_{Bi}\mu C_{ox}\frac{W_i}{L_i}}$ is the transconductance parameter of the i-th transistor (i = 1, 2, …, 8), I_{Bi} is the DC bias current, μ is the free carrier mobility, C_{ox} is the gate-oxide capacitance per unit area, and W_i and L_i are the effective channel width and length of the transistor M_i, respectively.

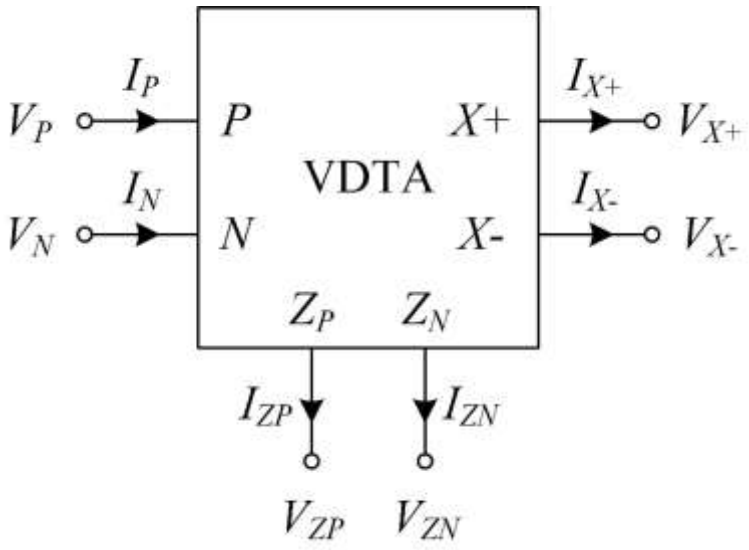

Fig. 1 The circuit symbol of the VDTA

The two-port network equation of an MCC shown in Fig. 2 is given below. Here, L_p and L_s represent the primary and secondary self-inductances, respectively.

$$\begin{bmatrix} V_1 \\ V_2 \end{bmatrix} = s \begin{bmatrix} L_p & M_{12} \\ M_{21} & L_s \end{bmatrix} \begin{bmatrix} I_1 \\ I_2 \end{bmatrix} \tag{4}$$

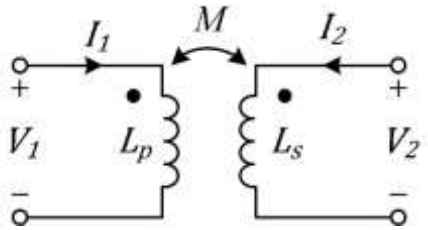

Fig. 2 Mutually coupled circuit

The equivalent circuit of the MCC is shown in Fig. 3. This equivalent circuit is expressed by the Eq. (5). M_{12} and M_{21} represent the mutually inductances. For symmetrical coupling the condition $M_{11} = M_{22} = M_{12} = M_{21} = M$ must be satisfied. According to Eqs. (4) and (5), $L_1 = L_p - M$, $L_2 = L_s - M$ and $L_3 = M$ are determined.

$$\begin{bmatrix} V_1 \\ V_2 \end{bmatrix} = s \begin{bmatrix} L_1 + M_{11} & M_{12} \\ M_{21} & L_2 + M_{22} \end{bmatrix} \begin{bmatrix} I_1 \\ I_2 \end{bmatrix} \tag{5}$$

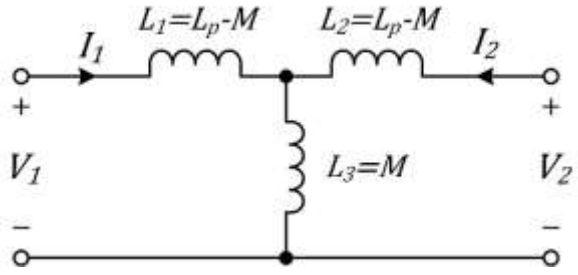

Fig. 3 The equivalent circuit

The proposed MCC is depicted in Fig. 4, and the two-port network equations are given in Eqs. (6) and (7).

$$V_1(s) = \frac{sC_1(1 + g_{mF1}R)}{g_{mF1}g_{mS1}} I_1(s) + \frac{sC_1R}{g_{mS1}} I_2(s) \tag{6}$$

$$V_2(s) = \frac{sC_2R}{g_{mS2}} I_1(s) + \frac{sC_2(1 + g_{mF2}R)}{g_{mF2}g_{mS2}} I_2(s) \tag{7}$$

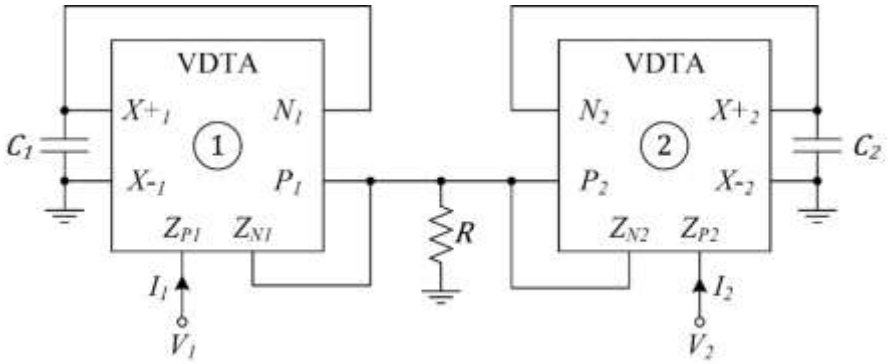

Fig. 4 The proposed MCC

The proposed MCC's inductance values are determined according to the Eqs. (4), (5), (6), and (7).

$$L_p = \frac{C_1(1 + g_{mF1}R)}{g_{mF1}g_{mS1}} \tag{8}$$

$$L_s = \frac{C_2(1 + g_{mF2}R)}{g_{mF2}g_{mS2}} \tag{9}$$

and

$$L_1 = \frac{C_1}{g_{mF1}g_{mS1}} \tag{10}$$

$$M_{11} = M_{12} = \frac{C_1R}{g_{mS1}} \tag{11}$$

$$L_2 = \frac{C_2}{g_{mF2}g_{mS2}} \tag{12}$$

$$M_{21} = M_{22} = \frac{C_2R}{g_{mS2}} \tag{13}$$

From Eqs. (8-13), it is clear that the inductances can be adjusted independently and electronically by the bias current of the VDTAs.

For the symmetrical coupling, the following condition should be met.

$$\frac{C_1}{g_{mS1}} = \frac{C_2}{g_{mS2}} \tag{14}$$

The coefficient of coupling is given by:

$$k = \sqrt{\frac{M_{12}M_{21}}{L_pL_s}} = \frac{R}{\sqrt{\left(\frac{1}{g_{mF1}} + R\right)\left(\frac{1}{g_{mF2}} + R\right)}} \tag{15}$$

3. Parasitic analysis

The VDTA including parasitic impedances are shown in Fig. 5. The port relations are given by:

$$\begin{bmatrix} I_P \\ I_N \\ I_{ZP} \\ I_{ZN} \\ I_{X_+} \\ I_{X_-} \end{bmatrix} = \begin{bmatrix} 0 & 0 & 0 & 0 & 0 & 0 \\ 0 & 0 & 0 & 0 & 0 & 0 \\ \beta_{FP}g_{mF} & -\beta_{FP}g_{mF} & 0 & 0 & 0 & 0 \\ -\beta_{FN}g_{mF} & \beta_{FN}g_{mF} & 0 & 0 & 0 & 0 \\ 0 & 0 & \beta_{SP}g_{mS} & 0 & 0 & 0 \\ 0 & 0 & -\beta_{SN}g_{mS} & 0 & 0 & 0 \end{bmatrix} \begin{bmatrix} V_P \\ V_N \\ V_{ZP} \\ V_{ZN} \\ V_{X_+} \\ V_{X_-} \end{bmatrix} \tag{16}$$

where β_{FP}, β_{FN}, β_{SP} and β_{SN} are the non-ideal transfer gains.

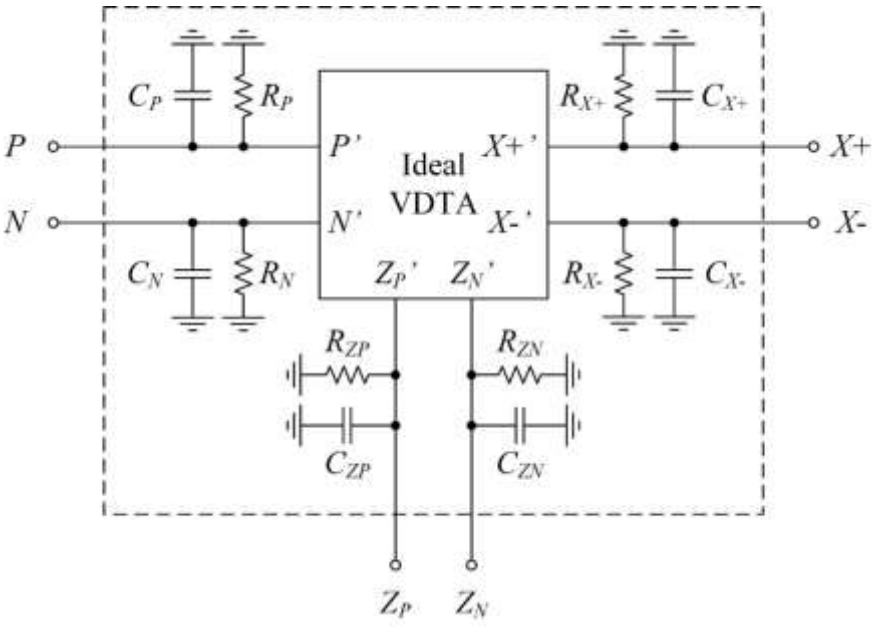

Fig. 5 The VDTA including parasitic impedances

If only the non-ideal transfer gains are taken into account, the following equations are obtained.

$$V_1(s) = \frac{sC_1(1+\beta_{FP1}g_{mF1}R)}{\beta_{FP1}g_{mF1}\beta_{SP1}g_{mS1}}I_1(s) + \frac{sC_1R}{\beta_{SP1}g_{mS1}}I_2(s) \tag{17}$$

$$V_2(s) = \frac{sC_2R}{\beta_{SP2}g_{mS2}}I_1(s) + \frac{sC_2(1+\beta_{FP2}g_{mF2}R)}{\beta_{FP2}g_{mF2}\beta_{SP2}g_{mS2}}I_2(s) \tag{18}$$

where β_{FPj}, β_{FNj}, β_{SPj} and β_{SNj} (j = 1, 2) are the corresponding non-ideal transfer gains of the jth VDTA.

The sensitivities of L_1, L_2, M_{11}, M_{12}, M_{21}, and M_{22} are given by the following equations. Note that the magnitude of the sensitivities is equal to unity.

$$S_{C_1}^{L_1} = -S_{\beta_{SP1}}^{L_1} = -S_{g_{mS1}}^{L_1} = 1 \tag{19}$$

$$S_{C_2}^{L_2} = -S_{\beta_{SP2}}^{L_2} = -S_{g_{mS2}}^{L_2} = 1 \tag{20}$$

$$S_{C_1}^{M_{11}} = S_R^{M_{11}} = -S_{\beta_{SP1}}^{M_{11}} = -S_{g_{mS1}}^{M_{11}} = 1 \tag{21}$$

$$S_{C_1}^{M_{12}} = S_R^{M_{12}} = -S_{\beta_{SP1}}^{M_{12}} = -S_{g_{mS1}}^{M_{12}} = 1 \tag{22}$$

$$S_{C_2}^{M_{21}} = S_R^{M_{21}} = -S_{\beta_{SP2}}^{M_{21}} = -S_{g_{mS2}}^{M_{21}} = 1 \tag{23}$$

$$S_{C_2}^{M_{22}} = S_R^{M_{22}} = -S_{\beta_{SP2}}^{M_{22}} = -S_{g_{mS2}}^{M_{22}} = 1 \tag{24}$$

If only the parasitic elements are considered, the following equations are derived.

$$V_1(s) = \frac{Y_1(\beta_{FP1}g_{mF1}+Y_3)}{\beta_{FP1}g_{mF1}\beta_{SP1}g_{mS1}Y_3}I_1(s) + \frac{Y_1}{\beta_{SP1}g_{mS1}Y_3}I_2(s) \tag{25}$$

$$V_2(s) = \frac{Y_2}{\beta_{SP2}g_{mS2}Y_3}I_1(s) + \frac{Y_2(\beta_{FP2}g_{mF2}+Y_3)}{\beta_{FP2}g_{mF2}\beta_{SP2}g_{mS2}Y_3}I_2(s) \tag{26}$$

where

$$Y_1 = s(C_1 + C_{X+1} + C_{N1}) + G_{X+1} + G_{N1} \tag{27}$$

$$Y_2 = s(C_2 + C_{X+2} + C_{N2}) + G_{X+2} + G_{N2} \tag{28}$$

$$Y_3 = s(C_{P1} + C_{ZN1} + C_{P2} + C_{ZN2}) + G + G_{P1} + G_{ZN1} + G_{P2} + G_{ZN2} \tag{29}$$

Comparing Eqs. (4), (5), (25), and (26), the inductances are found as:

$$sL_P = \frac{Y_1(\beta_{FP1} g_{mF1} + Y_3)}{\beta_{FP1} g_{mF1} \beta_{SP1} g_{mS1} Y_3} \tag{30}$$

$$sL_S = \frac{Y_2(\beta_{FP2} g_{mF2} + Y_3)}{\beta_{FP2} g_{mF2} \beta_{SP2} g_{mS2} Y_3} \tag{31}$$

$$sL_1 = \frac{Y_1}{\beta_{FP1} g_{mF1} \beta_{SP1} g_{mS1}} \tag{32}$$

$$sM_{11} = sM_{12} = \frac{Y_1}{\beta_{SP1} g_{mS1} Y_3} \tag{33}$$

$$sL_2 = \frac{Y_2}{\beta_{FP2} g_{mF2} \beta_{SP2} g_{mS2}} \tag{34}$$

$$sM_{21} = sM_{22} = \frac{Y_2}{\beta_{SP2} g_{mS2} Y_3} \tag{35}$$

The coefficient of coupling is obtained in non-ideal conditions.

$$k = \sqrt{\frac{M_{12} M_{21}}{L_p L_s}} = \frac{1}{\sqrt{\left(1 + \frac{Y_3}{\beta_{FP1} g_{mF1}}\right)\left(1 + \frac{Y_3}{\beta_{FP2} g_{mF2}}\right)}} \tag{36}$$

If only parasitic impedances of the P and Z_N terminals are considered, the following condition must be satisfied. The inequality given in Eq. (37) can be written as in Eq. (38) with an acceptable error.

$$\left|(R_{P1} \parallel R_{ZN1} \parallel R_{P2} \parallel R_{ZN2}) \parallel \frac{1}{j\omega(C_{P1} + C_{ZN1} + C_{P2} + C_{ZN2})}\right| \gg R \tag{37}$$

$$\left|(R_{P1} \parallel R_{ZN1} \parallel R_{P2} \parallel R_{ZN2}) \parallel \frac{1}{j\omega(C_{P1} + C_{ZN1} + C_{P2} + C_{ZN2})}\right| \geq 10 \times R \tag{38}$$

The following inequality is derived by using Eq. (38).

$$\frac{(R_{P1} \parallel R_{ZN1} \parallel R_{P2} \parallel R_{ZN2})}{\sqrt{1 + \omega^2(R_{P1} \parallel R_{ZN1} \parallel R_{P2} \parallel R_{ZN2})^2(C_{P1} + C_{ZN1} + C_{P2} + C_{ZN2})^2}} \geq 10 \times R \tag{39}$$

In Eq. (39), if R_{P1}, R_{ZN1}, R_{P2} and R_{ZN2} are ignored, the inequality in Eq. (40) is obtained. The upper operating frequency limit of the circuit is obtained approximately as in Eq. (41).

$$\left|\frac{1}{\omega(C_{P1} + C_{ZN1} + C_{P2} + C_{ZN2})}\right| \geq 10 \times R \tag{40}$$

$$\omega \leq \frac{1}{10 \times R \times (C_{P1} + C_{ZN1} + C_{P2} + C_{ZN2})} = \omega_H \tag{41}$$

In Eq. (39), if C_{P1}, C_{ZN1}, C_{P2} and C_{ZN2} are ignored, R must satisfy the following condition.

$$(R_{P1} \parallel R_{ZN1} \parallel R_{P2} \parallel R_{ZN2}) \geq 10 \times R \tag{42}$$

If only parasitic impedances of the N and $X+$ terminals are considered, the inequality in Eq. (43) must be satisfied. Eq. (43) can be written as in Eq. (44).

$$\left|(R_{X+1} + R_{N1}) \parallel \frac{1}{j\omega(C_{X+1} + C_{N1})}\right| \gg \left|\frac{1}{j\omega C_1}\right| \tag{43}$$

$$\left|(R_{X+1}+R_{N1}) \parallel \frac{1}{j\omega(C_{X+1}+C_{N1})}\right| \geq 10 \times \left|\frac{1}{j\omega C_1}\right| \tag{44}$$

The following inequality is derived by using Eq. (43).

$$\frac{(R_{X+1}+R_{N1})}{\sqrt{1+\omega^2(R_{X+1}+R_{N1})^2(C_{X+1}+C_{N1})^2}} \geq \frac{10}{\omega C_1} \tag{45}$$

In Eq. (45), if R_{X+1} and R_{N1} are ignored, C_1 must satisfy the following condition.

$$C_1 \geq 10 \times (C_{X+1}+C_{N1}) \tag{46}$$

In Eq. (45), if C_{X+1} and C_{N1} are ignored, the inequality in Eq. (47) is obtained. The lower operating frequency limit of the circuit is obtained approximately as in Eq. (48).

$$(R_{X+1}+R_{N1}) \geq \frac{10}{\omega C_1} \tag{47}$$

$$\omega \geq \frac{10}{(R_{X+1}+R_{N1})C_1} = \omega_{L1} \tag{48}$$

A similar analysis for the second VDTA yields the following results.

$$C_2 \geq 10 \times (C_{X+2}+C_{N2}) \tag{49}$$

$$(R_{X+2}+R_{N2}) \geq \frac{10}{\omega C_2} \tag{50}$$

$$\omega \geq \frac{10}{(R_{X+2}+R_{N2})C_2} = \omega_{L2} \tag{51}$$

The operating frequency limits are obtained as follows.

$$max\{\omega_{L1}, \omega_{L2}\} \leq \omega \leq \omega_H \quad (52)$$

The effects of parasitic impedances can be reduced by applying the following design criteria.

1. The total admittance connected to $X+_1$ and N_1 terminals of the first VDTA is given in Eq. (27). If the capacitor C_1 is chosen much larger than other parasitic elements, the total impedance will be C_1. Capacitor C_1 must meet the condition $C_1 \geq 10$ x ($C_{X+1} + C_{N1}$).

2. For the second VDTA, the total admittance connected to $X+_2$ and N_2 terminals is given in Eq. (28). If the capacitor C_2 is chosen much larger than the other parasitic impedances, the total impedance will be equal to C_2. C_2 must satisfy the condition $C_2 \geq 10$ x ($C_{X+2} + C_{N2}$).

3. The total admittance connected to P_1, Z_{N1}, P_2 and Z_{N2} is given in Eq. (29). The resistor R should be chosen small enough to meet the condition ($R_{P1} \parallel R_{ZN1} \parallel R_{P2} \parallel R_{ZN2}$) ≥ 10 x R.

4. Application example

A DTBP filter is given to demonstrate the functionality of the circuit. The filter is constructed by using additionally two resistors and two capacitors. The circuit schematic is given in Fig. 6. The angular resonant frequencies (ω_p and ω_s) and the quality factors (Q_p and Q_s) are given by:

$$Q_p = \omega_p C_p R_p \quad (53)$$

$$Q_s = \omega_s C_s R_s \quad (54)$$

$$\omega_p = \frac{1}{\sqrt{C_p L_p}} \quad (55)$$

$$\omega_s = \frac{1}{\sqrt{C_s L_s}} \quad (56)$$

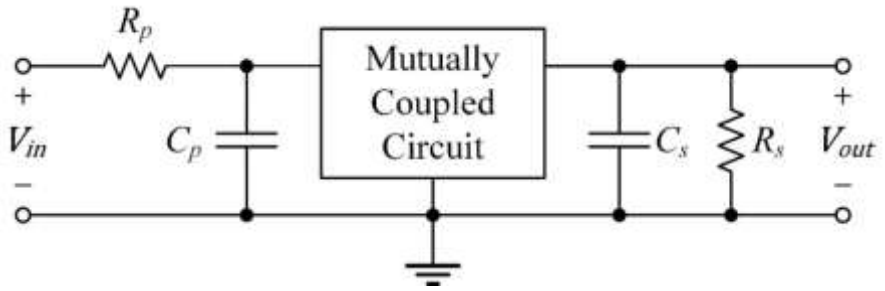

Fig. 6 Double-tuned band-pass filter

5. Simulation results

LTspice program has been used for verifying simulation of the proposed VDTA based MCC with TSMC 0.18 μm CMOS technology parameters. The enhancement VDTA configuration is shown in Fig. 7 as CMOS implementation. Aspect ratios of the transistors are demonstrated in Table 2. The DC power supplies of structure are given $V_{DD} = -V_{SS} = 0.9V$, $V_{B1} = -V_{B2} = V_{B3} = -V_{B4} = 0.2$ V and the value of bias current sources are taken $I_{B1} = I_{B2} = I_{B3} = I_{B4} = I_{bias} = 300$ μA in the begining.

In order to simulate the proposed MCC, the DTBP filter has been used. The circuit of DTBP filter is shown in Fig. 6. LTspice simulation results are given in Fig. 8, together proposed VDTA based circuit and ideal structure. To achieve this solution, the passive elements has been selected as $C_p = C_s = 100$ pF, $R_p = R_s = 5$ kΩ, $C_1 = C_2 = 280$ pF and R = 422.83 Ω because of attaining the inductances as $L_p = L_s = 100$ μH and $M_{11} = M_{22} = M_{12} = M_{21} = M = L_1 = L_2 = 50$ μH. With these selections, other paramaters are obtained as k = 0.5, $w_p = w_s = 10$ Mrad/s, $Q_p = Q_s = 5$. By altering the values of the passive components as $C_p = C_s = 1$ nF, $R_p = R_s = 10$ kΩ, $C_1 = C_2 = 280$ pF and R = 422.83 Ω in order to attain the inductances as $L_p = L_s = 1$ mH and $M_{11} = M_{22} = M_{12} = M_{21} = M = L_1 = L_2 = 500$ μH, changing in the simulation results can be observed in Fig. 9. In this observation the other paramaters are k = 0.5, $w_p = w_s = 1$ Mrad/s, $Q_p = Q_s = 10$. To show the effect of coefficient of coupling (k) on the DTBP filter, another simulation has been executed. Alteration of the frequency response on simulation results are shown in Fig. 10, with different values of coefficient of coupling (k). In this experience, coefficient of coupling has been taken as k = 0.2 (R = 105.7 Ω), k = 0.4 (R = 281.89 Ω), k = 0.6 (R = 634.245 Ω), k = 0.8 (R = 1691.32 Ω), respectively.

To illustrate of electronically tunability of the proposed MCC, the bias current that $I_{B1} = I_{B2} = I_{B3} = I_{B4} = I_{bias}$ is altered as $I_{bias} = 300$ μA, $I_{bias} = 400$ μA and $I_{bias} = 500$ μA while the passive components has been taken as $C_p =$

C_s = 100 pF, R_p = R_s = 5 kΩ, C_1 = C_2 = 280 pF and R = 422.83 Ω and consequently L_p = L_s = 100 µH and M_{11} = M_{22} = M_{12} = M_{21} = M = L_1 = L_2 = 50 µH equations are obtained. Frequency response of this alteration is shown in Fig. 11.

Monte Carlo (MC) analysis has been executed hundered times to achieve the mismatch on the frequency response of the proposed circuit by uniformly altered of passive components as 5%, thickness (t_{ox}) and treshold voltages (V_{TH}) as %20 and supply voltages as %20. Simulation of the MC analysis results are given in Fig. 12, Fig. 13 and Fig. 14 as frequency response. On the other hand, to show maximum gain of the variations, histograms are given in Fig. 15, Fig. 16 and Fig. 17.

In order to show the distortion of the proposed MCC, THD analysis has been realised. With changing of the input peak voltages, the THD percentage is given in Fig. 18. In this simulation, input peak voltage has been altered 0 to 400 mV. Besides, frequency of the signal has been selected as 1.59 MHz. Maximum value of the THD detemined as 0.56% at 40 mV in this simulation.

Response of the proposed MCC respect to alter of the temperature has been investigated. Simulation results of this investigation is given in Fig. 19. Temperture has been changed range of the -50 to 100 °C by incrementing 50 °C.

Output noise alteration of the proposed MCC has been illustrated respect to frequency changing in Fig. 20.

Input and output time domain analysis of the DTBP filter that designed with VDTA based MCC is given in Fig. 21. The input signal that has 100 mV peak voltage and 1.59 MHz frequency is sinusoidal. In this analysis it can be determined that there is no substantial difference between simulated and ideal output signals.

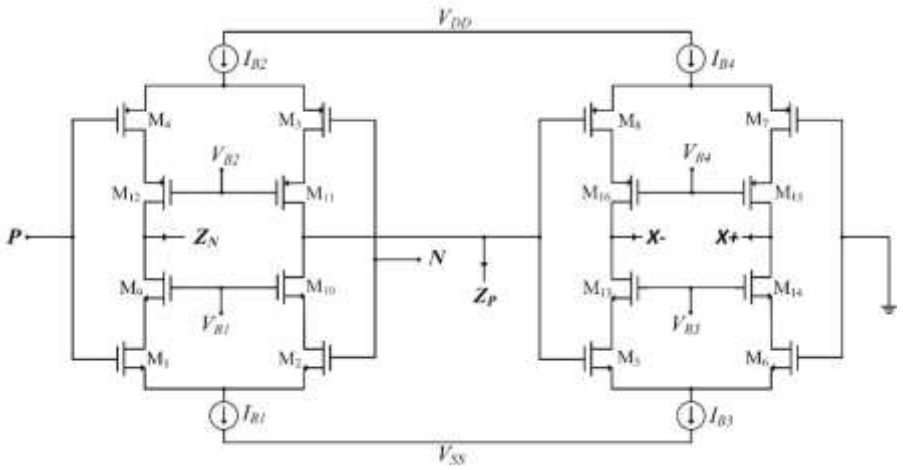

Fig. 7 The internal structure of the VDTA [19], [20]

Table 2 Aspect ratios of transistors [20]

Transistor names	W(μm)	L(μm)
M_1, M_2, M_5, M_6	18	0.18
M_3, M_4, M_7, M_8	72	0.18
M_9, M_{10}, M_{13}, M_{14}	27	0.18
M_{11}, M_{12}, M_{15}, M_{16}	90	0.18

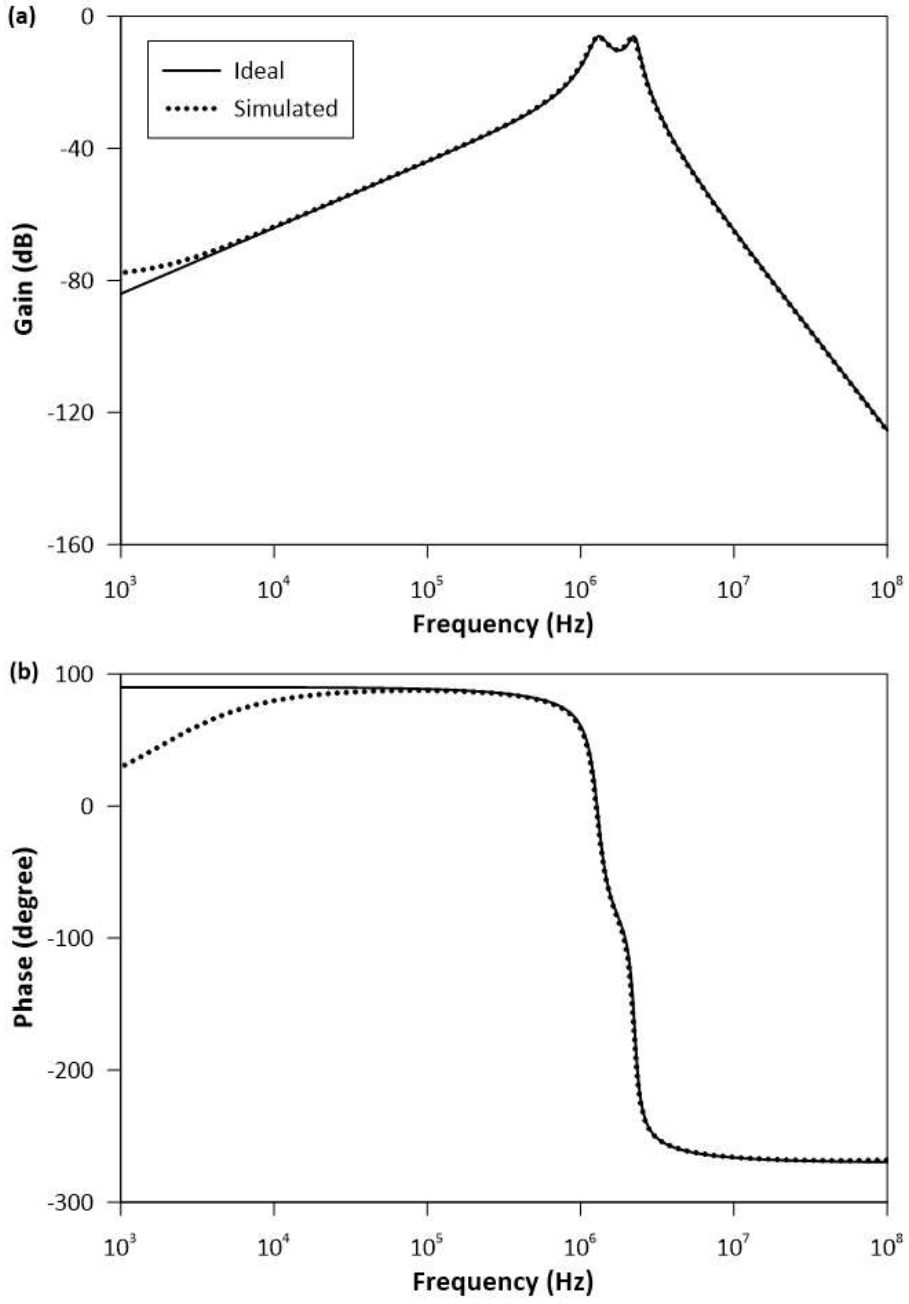

Fig 8 Ideal and simulated frequency response of the DTBP filter where k = 0.5, $w_p = w_s = 10$ Mrad/s, $Q_p = Q_s = 5$. **a** Magnitude, **b** phase response.

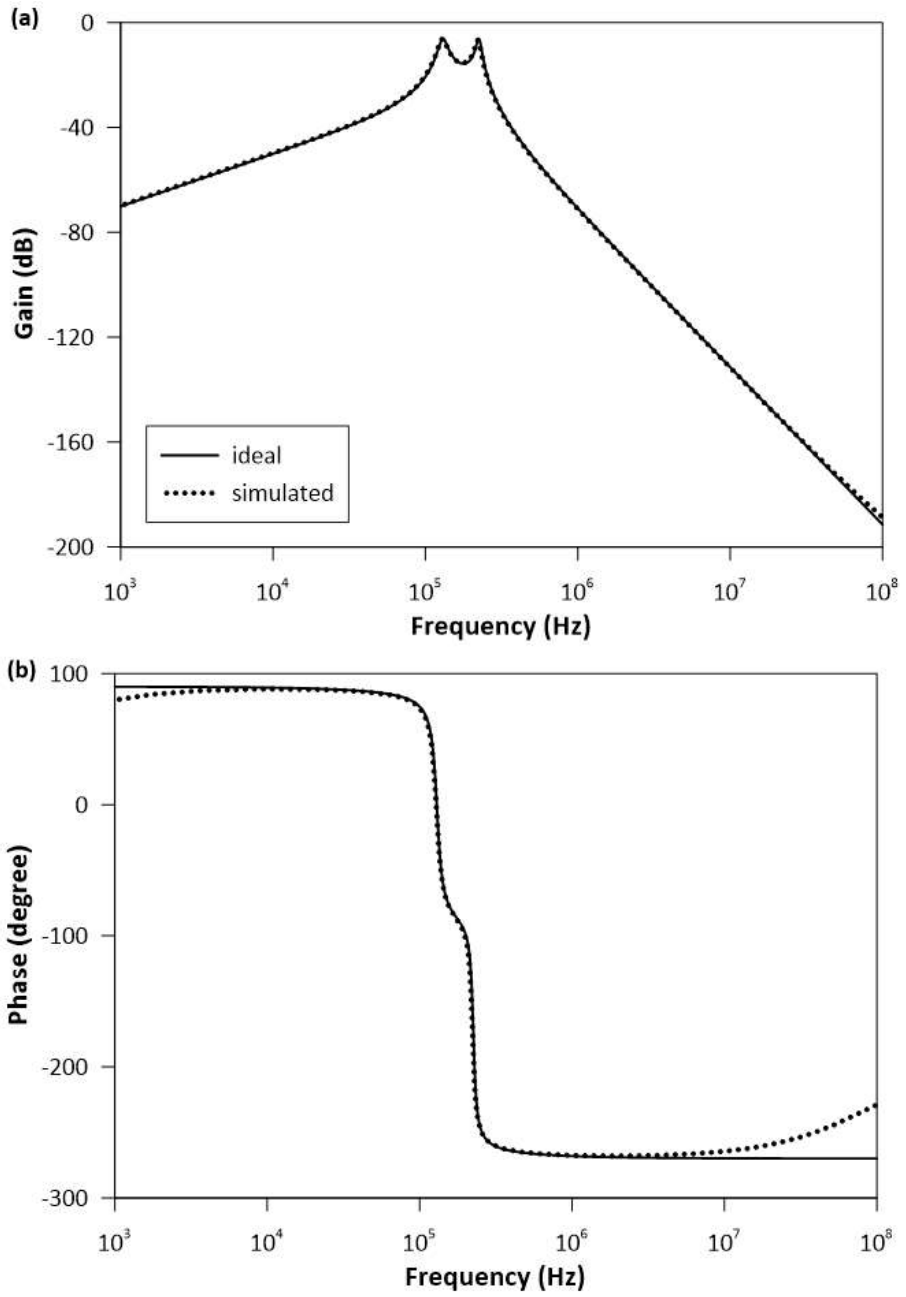

Fig. 9 Ideal and simulated frequency response of the DTBP filter where k = 0.5, $w_p = w_s = 1$ Mrad/s, $Q_p = Q_s = 10$. **a** Magnitude, **b** phase response.

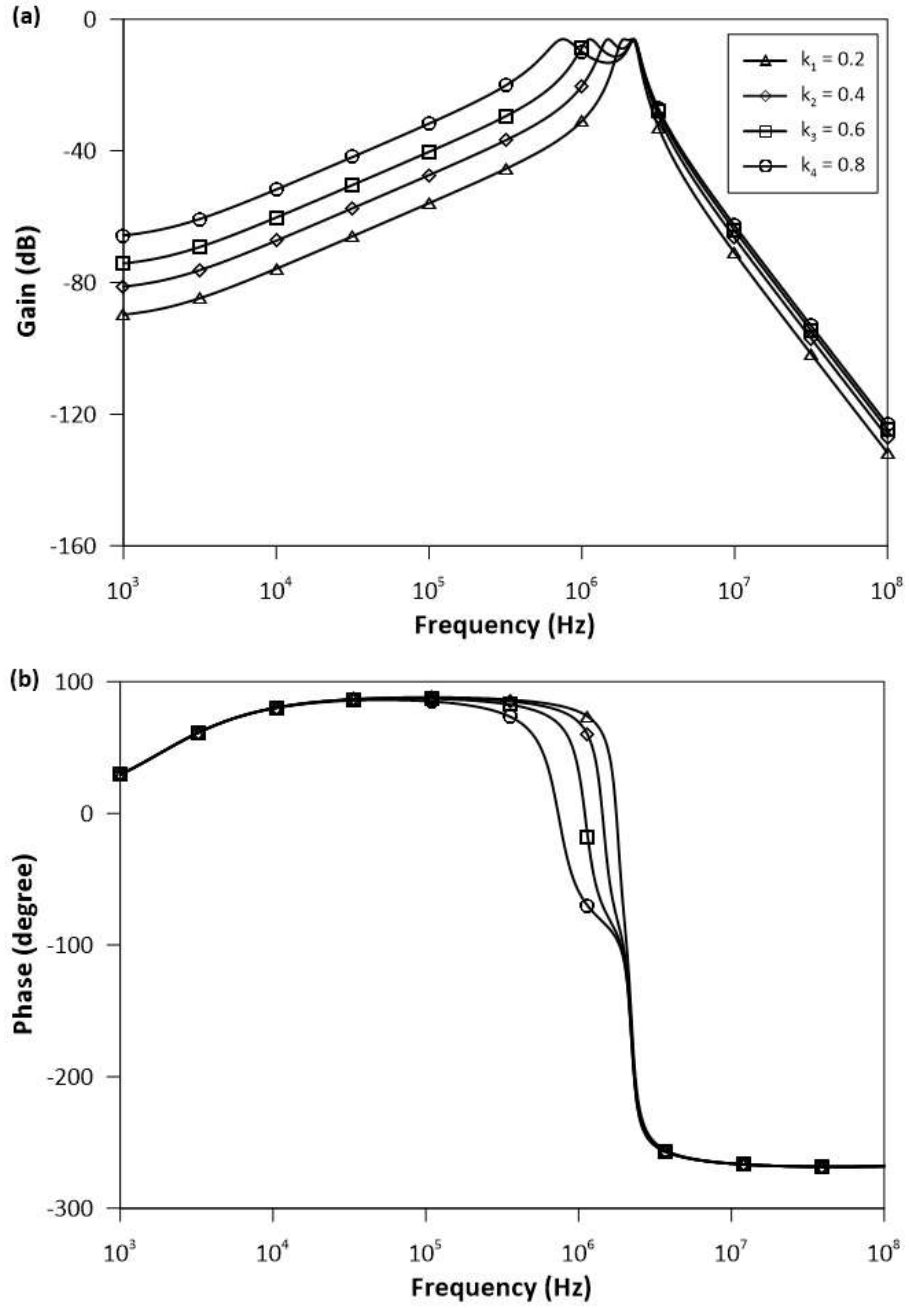

Fig. 10 Frequency response of the DTBP filter where k = 0.2, 0.4, 0.6 and $w_p = w_s = 10$ Mrad/s, $Q_p = Q_s = 5$. **a** Magnitude, **b** phase response.

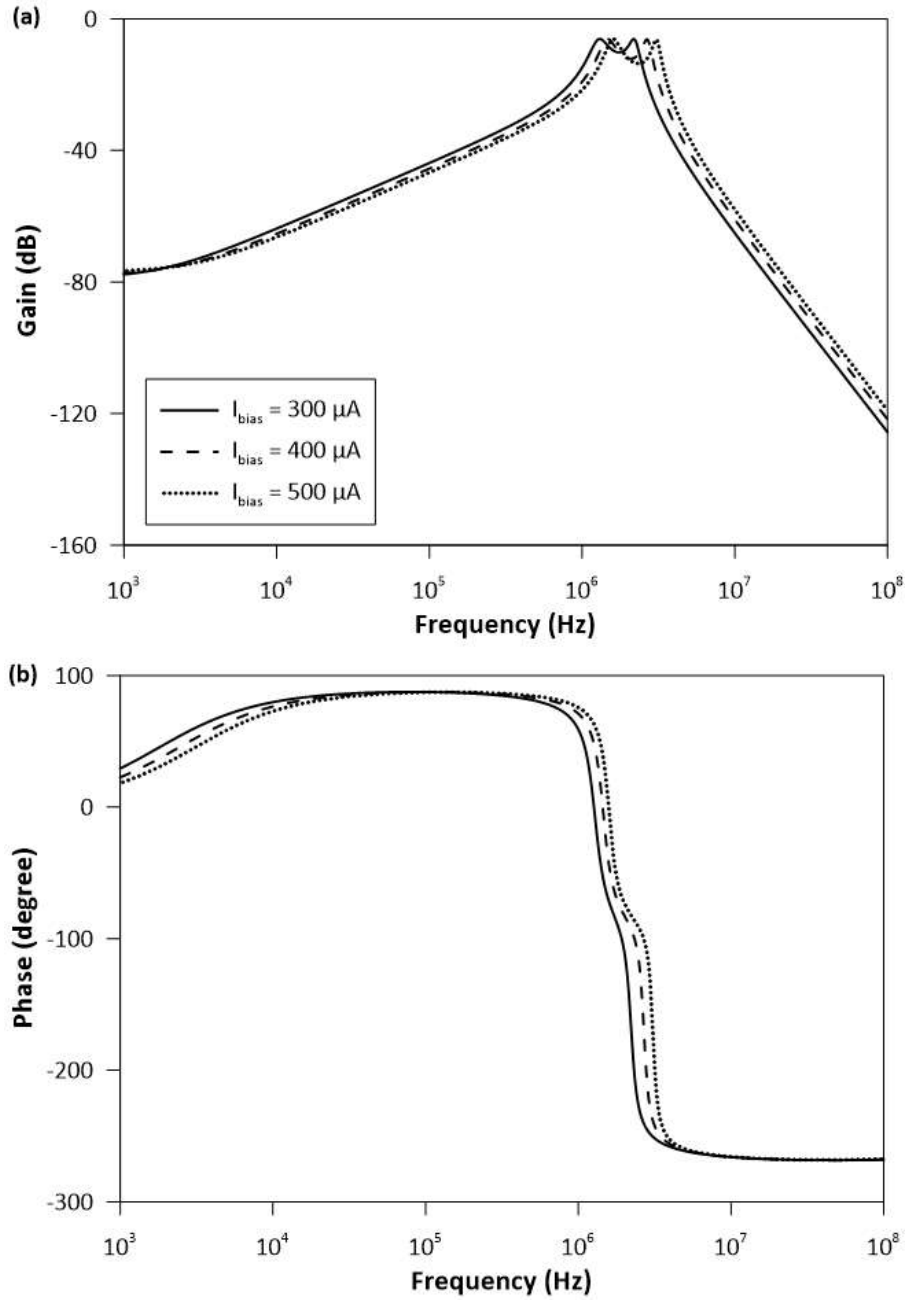

Fig. 11 Frequency response of the DTBP filter where I_{bias} = 300 µA, 400 µA, 500 µA, k = 0.5, $w_p = w_s$ = 10 Mrad/s, $Q_p = Q_s$ = 5. **a** Magnitude, **b** phase response.

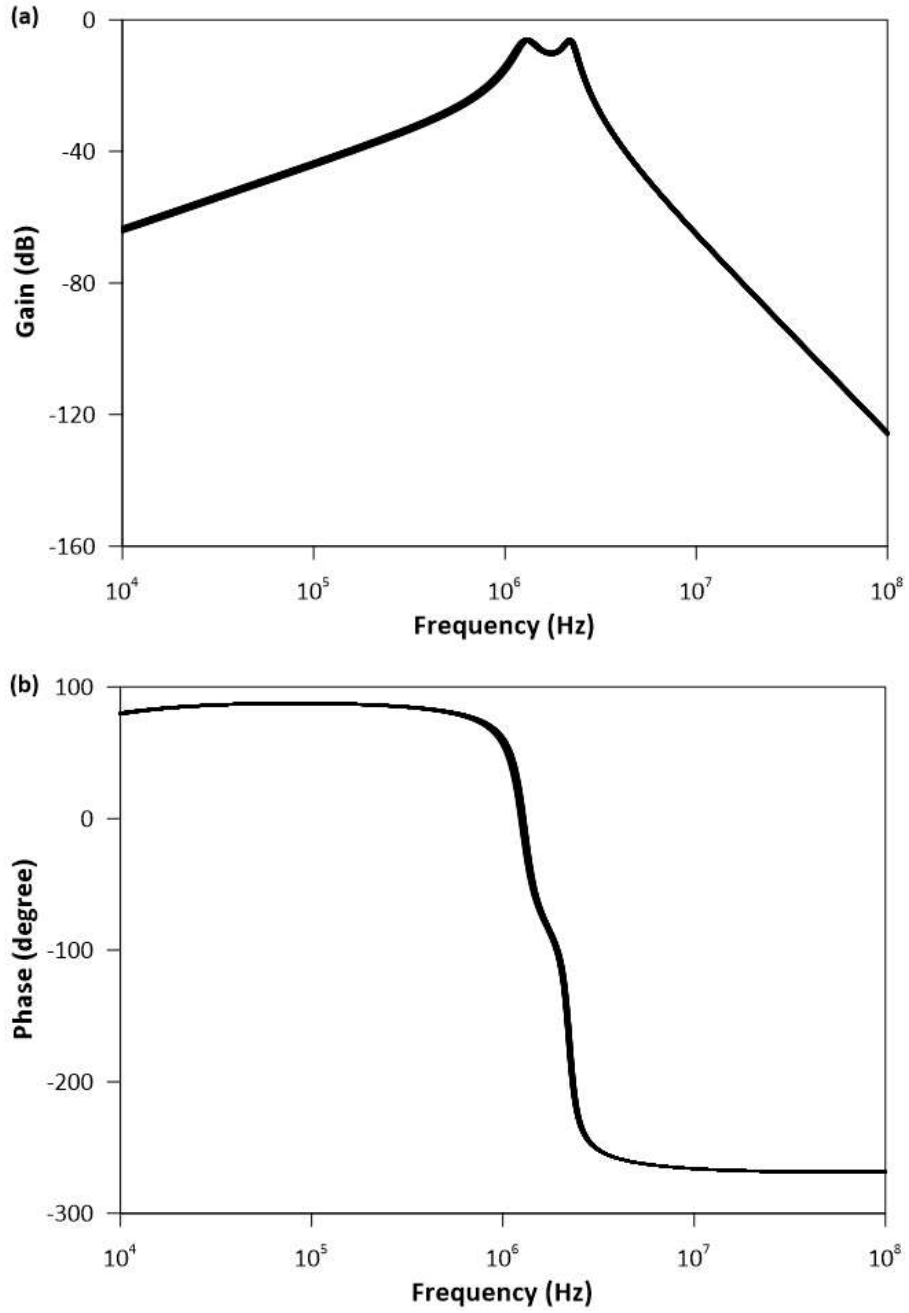

Fig. 12 Monte Carlo analysis results of the DTBP filter that has been run one hundred times by uniformly altered of passive components as 5% where k = 0.5, $w_p = w_s = 10$ Mrad/s, $Q_p = Q_s = 5$. **a** Magnitude, **b** phase response.

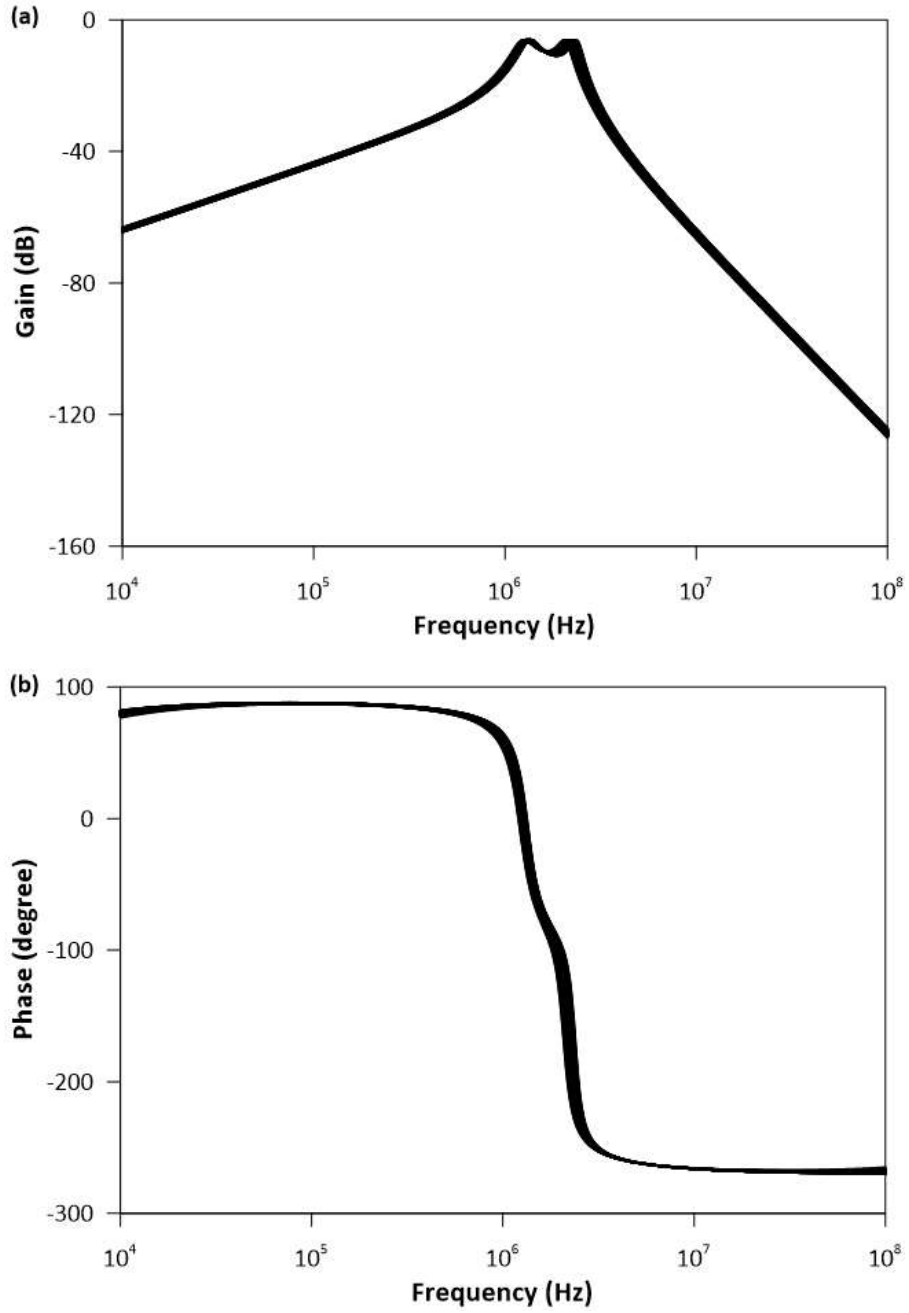

Fig. 13 Monte Carlo analysis results of the DTBP filter that has been run one hundred times by uniformly altered of t_{ox} and V_{TH} as 20% where k = 0.5, $w_p = w_s$ = 10 Mrad/s, $Q_p = Q_s = 5$. **a** Magnitude, **b** phase response.

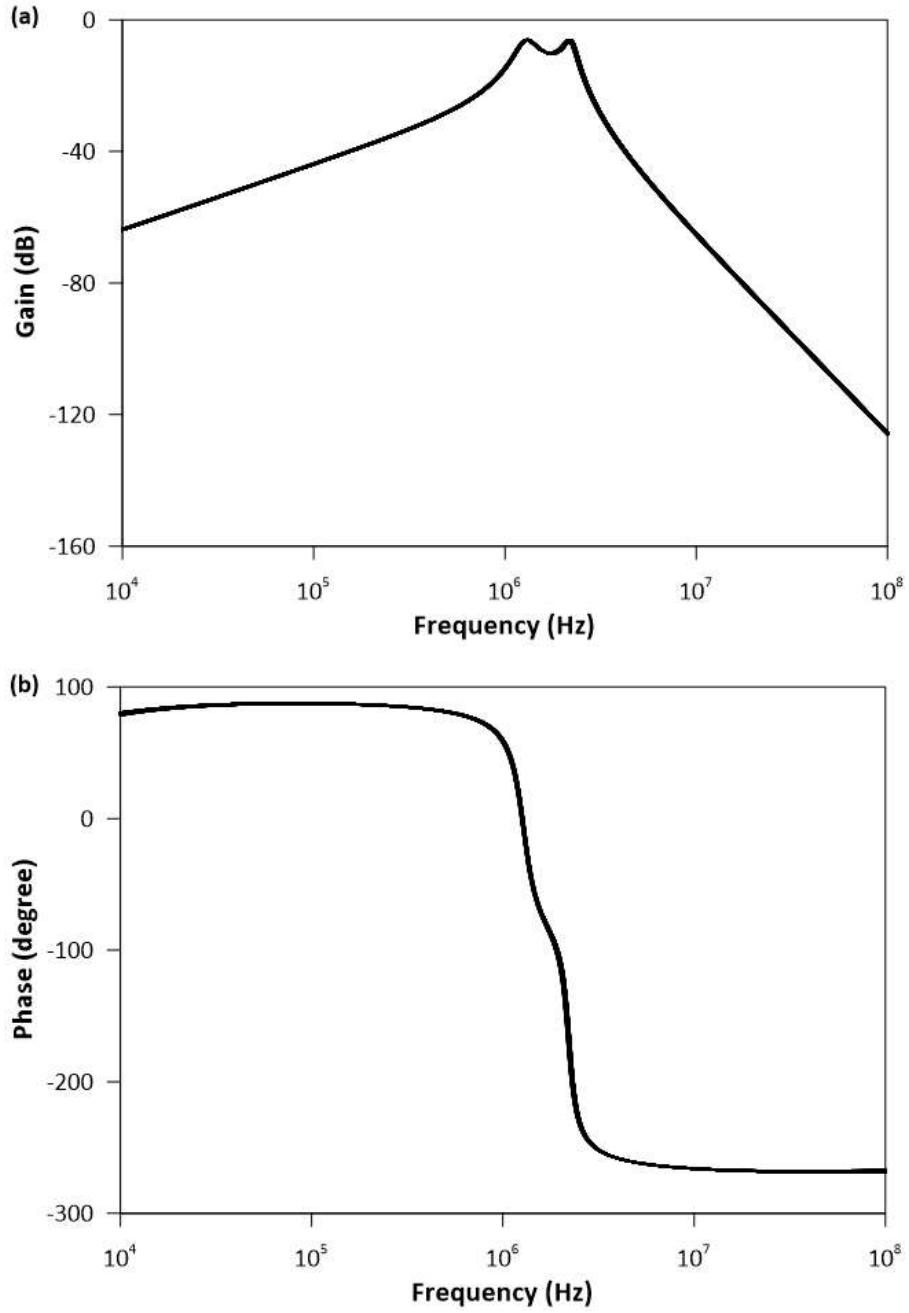

Fig. 14 Monte Carlo analysis results of the DTBP filter that has been run one hundred times by uniformly altered of supply voltages as 20% where k = 0.5, $w_p = w_s = 10$ Mrad/s, $Q_p = Q_s = 5$. **a** Magnitude, **b** phase response.

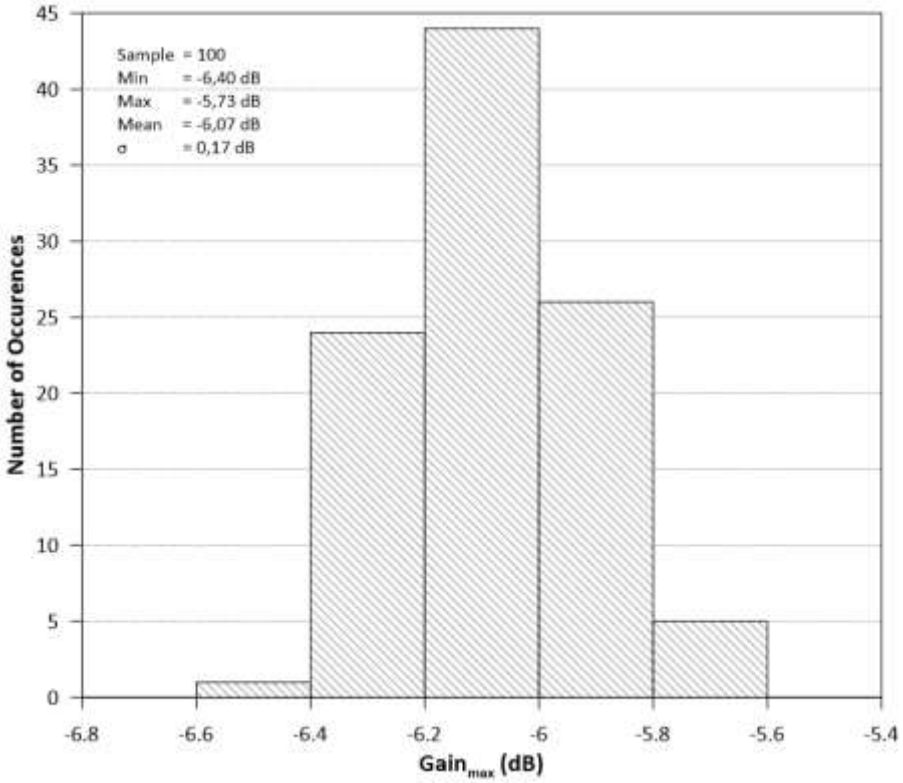

Fig. 15 Maximum gain histogram of the DTBP filter by uniformly altered of passive components as 5% where k = 0.5, $w_p = w_s = 10$ Mrad/s, $Q_p = Q_s = 5$.

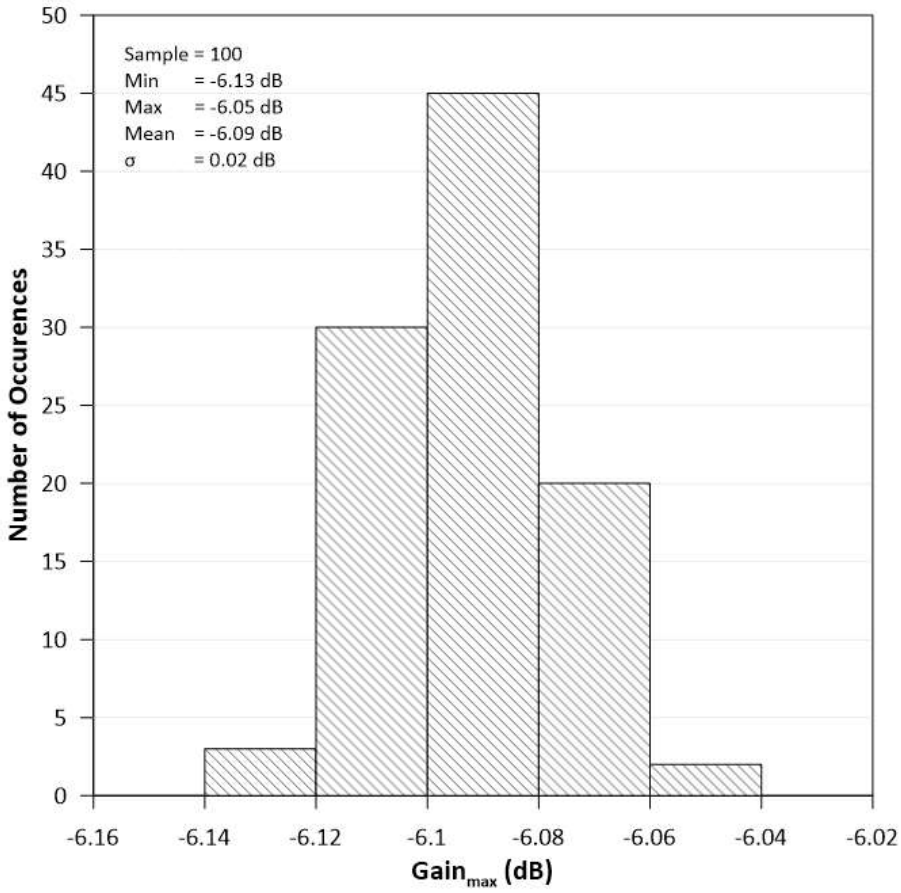

Fig. 16 Maximum gain histogram of the DTBP filter by uniformly altered of t_{ox} and V_{TH} as 20% where k = 0.5, $w_p = w_s = 10$ Mrad/s, $Q_p = Q_s = 5$.

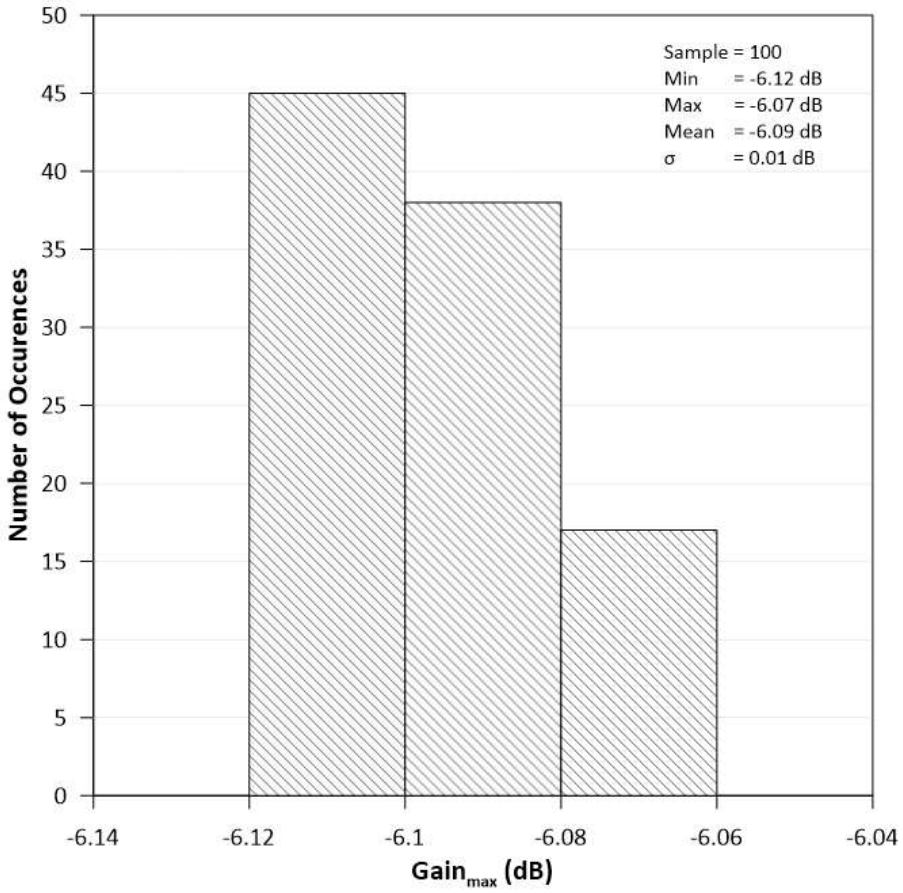

Fig. 17 Maximum gain histogram of the DTBP filter by uniformly altered supply voltages as 20% where k = 0.5, $w_p = w_s = 10$ Mrad/s, $Q_p = Q_s = 5$.

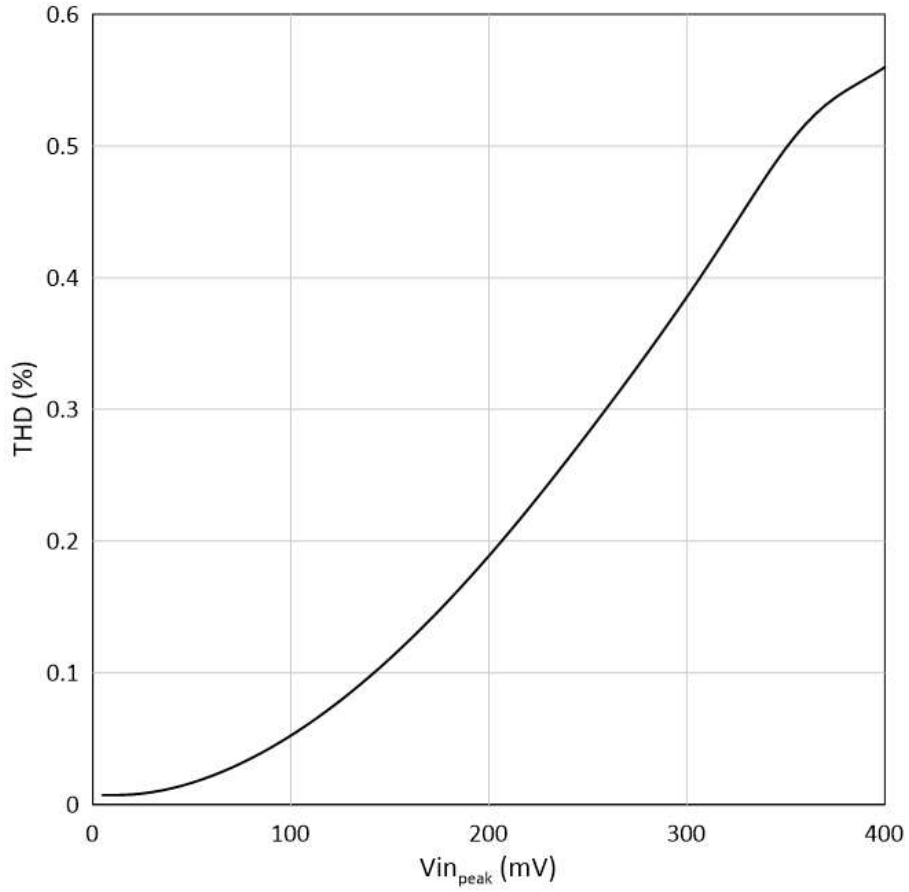

Fig. 18 Total harmonic distortion (THD) analysis of the DTBP filter with input peak voltages.

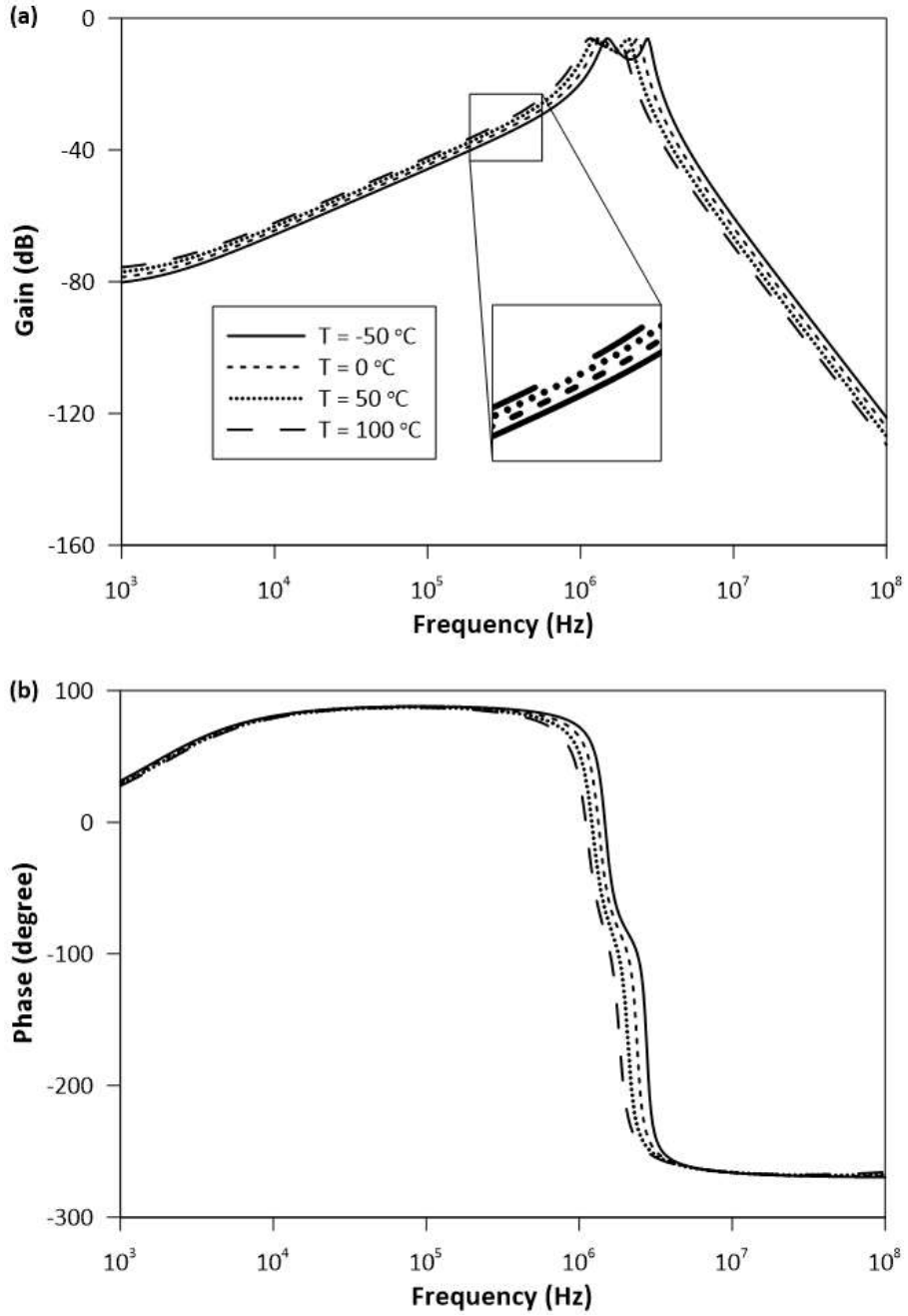

Fig. 19 Frequency response of DTBP filter with temperature changing where k = 0.5, $w_p = w_s = 10$ Mrad/s, $Q_p = Q_s = 5$. **a** Magnitude, **b** phase response.

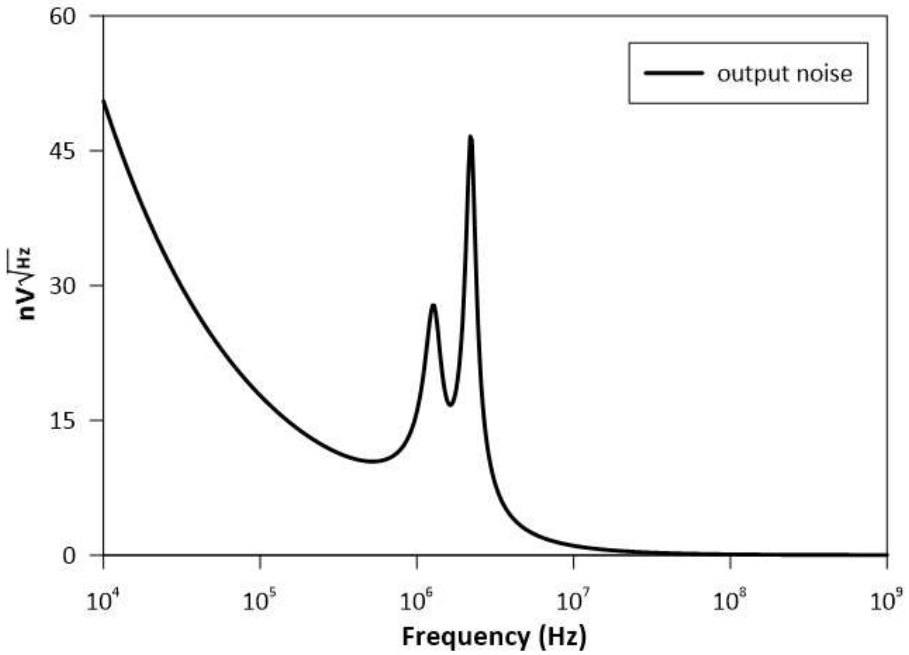

Fig. 20 Output noise alteration of the DTBP filter respect to frequency changing where k = 0.5, $w_p = w_s = 10$ Mrad/s, $Q_p = Q_s = 5$.

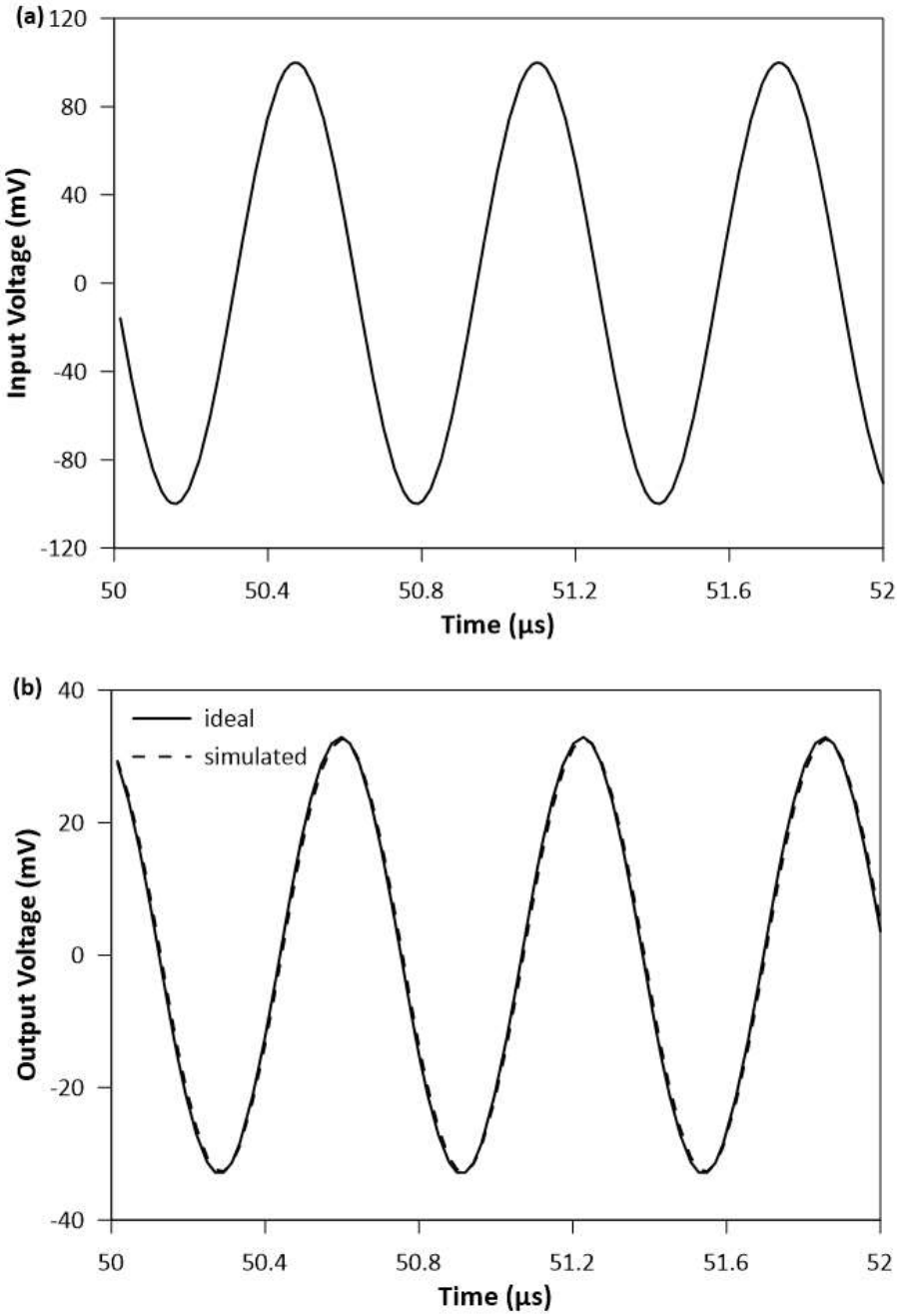

Fig. 21 Transient analysis of the DTBP filter. **a** Input, **b** simulated and ideal output results.

6. Conclusion

In this paper, a novel MCC, namely synthetic transformer has been presented. The proposed circuit includes two VDTAs, two grounded capacitors, and a resistor. The inductances can be controlled independently / electronically by bias current of VDTAs. There is only one matching condition to providing symmetrical coupling. The simulation results show the functionality of the proposed MCC.

Data availability statement

The datasets generated during and/or analyzed during the current study are available from

the corresponding author on reasonable request.

Funding information

The author(s) received no specific funding for this work.

Conflict of interest

The authors declared that there is no conflict of interest.

References

1. Atiya, F. (1978). The composite active filter: A combined wave active and gyrator-C filter. IEEE Transactions on Circuits Systems, 25, 573–579.
2. Soderstrand, M. (1978). Active R ladders: High frequency, high order, low sensitivity active R filters without external capacitors. IEEE Transactions on Circuits Systems, 25, 1032–1038.
3. Higashimura, M., & Fukui, Y. (1985). Realization of new mutually coupled circuits using mutators. International Journal of Electronics, 58, 477–485.
4. Higashimura, M., & Fukui, Y. (1991). Electronically tunable OTA-C mutually coupled circuit. Electronics Letters, 27, 1251.
5. Higashimura, M., & Fukui, Y. (1991). RC active realization of mutually coupled circuit. In IEEE International sympoisum circuits systems (vol. 3, pp. 1343–1346). IEEE.
6. Shigehiro, T., Nakamura, M., & Yoneda, S. (1991). A simulation of high-frequency mutually coupled circuit using bipolar transistors. Electron Commun Japan (Part II Electron), 74, 74–83.
7. Nakamura, M., Okine, M., Shigehiro, T., & Unehara, T. (1996). A synthesis of an LC simulation-Type double-tuned circuit adjustable by a single parameter. Electron Commun Japan (Part II Electron), 79, 66–75.
8. Taher Abuelma'atti, M., Muhammad Al-Shahrani, S., & Kulaib Al-Absi, M. (2005). Simulation of a mutually coupled circuit using plus-type CCIIs. International Journal of Electronics, 92, 49–54.

9. Yuce, E., Minaei, S., & Ibrahim, M. A. (2007). A new simulation of mutually coupled circuit based on CCIIs. International Journal of Electronics, 94, 367–372.
10. Yuce, E., & Minaei, S. (2007). A New active network suitable for realizing ladder filters and transformer simulator. Journal of Circuits, Systems and Computers, 16, 29–41.
11. Yuce, E., & Minaei, S. (2008). Electronically tunable simulated transformer and its application to stagger-tuned filter. IEEE Transactions on Instrumentation and Measurement, 57, 2083–2088.
12. Gunes, E. O., Zeki, A., & Toker, A. (2011). Design of a high performance mutually coupled circuit. Analog Integrated Circuits and Signal Processing, 66, 81–91.
13. Koksal, M., Ayten, U. E., & Sagbas, M. (2012). Realization of new mutually coupled circuit using CC-CBTAs. Circuits, Systems and Signal Processing, 31, 435–446.
14. Pandey, N., Arora, S., Takkar, R., & Pandey, R. (2012). DVCCCTA-based implementation of mutually coupled circuit. ISRN Electron, 2012, 1–6.
15. Sagbas, M. (2014). Electronically tunable mutually coupled circuit using only two active components. International Journal of Electronics, 101, 364–374.
16. Sagbas, M., Ayten, U. E., Sedef, H., & Minaei, S. (2017). Modified Gorski–Popiel technique and synthetic floating transformer circuit using minimum components. Journal of Circuits, Systems and Computers, 26, 1750013.
17. Dogan, M., Yuce, E., Minaei, S., & Sagbas, M. (2020). Synthetic transformer design using commercially available active components. Circuits, Systems and Signal Processing, 39, 3770–3786.
18. Ozer, E., & Kacar, F. (2021). On the realization of electronically tunable mutually coupled circuit employing voltage differencing current conveyors (VDCCs). Analog Integrated Circuits and Signal Processing, 110 (2), 289-300.
19. Yeşil, A., Kaçar, F., & Kuntman, H. (2011). New simple CMOS realization of voltage differencing transconductance amplifier and its RF filter application. Radioengineering, 20 (3), 632-637.
20. Yeşil, A., & Kaçar, F. (2013) - Electronically tunable resistorless mixed mode biquad filters Radioengineering, 22 (4), 1016-1025.